High power, tunable hybrid fiber/bulk laser at 1030 nm and parametric frequency conversion in the near and mid-infrared

Thomas Hamoudi, Marie Guionie, Xavier Delen, Jean-Baptiste Dherbecourt, Jean-Michel Melkonian, Antoine Godard, Myriam Raybaut, Patrick Georges

Applied Physics B manuscript No.
(will be inserted by the editor)

High power, tunable hybrid fiber/bulk laser at 1030 nm and parametric frequency conversion in the near and mid-infrared

T. Hamoudi[1], M. Guionie[1], X. Delen[2] ⋆, J.-B. Dherbecourt[1], J.-M. Melkonian[1], A. Godard[1], M. Raybaut[1], P. Georges[2]

[1] DPHY, ONERA, Université Paris-Saclay, F-91123 Palaiseau, France
[2] Université Paris-Saclay, Institut d'Optique Graduate School, CNRS, Laboratoire Charles Fabry, 91127 Palaiseau, France

Received: date / Revised version: date

Abstract We report on a high power, wavelength-agile, hybrid fiber-bulk laser, emitting up to 3.5 mJ 15 ns pulses at 1030 nm at 5 kHz repetition rate. This hybrid laser is composed of a commercial seed single-frequency fiber laser, tunable over several GHz, amplified in a dual-stage single-mode Ytterbium doped fiber amplifier, followed by two Yb:YAG solid crystal amplifiers. In order to illustrate the potential of such an architecture for future differential absorption lidar emitters, this hybrid source was used to pump an optical parametric amplifier (OPA) seeded by the idler at 3 µm generated by a fixed nested cavity optical parametric oscillator (NesCOPO). The wavelength agility of the pump is transferred to the OPA signal beam in order to reach a fine tunability in the 1.5 µm region. This fine tuning was used to measure the transmission spectrum of an acetylene gas cell.

1 Introduction

Pulsed, kHz repetition rate, nanosecond coherent sources, emitting energies in the hundreds of microjoules to millijoules levels are of high interest for remote sensing applications. In the frame of Differential Absorption LIDAR (DIAL) developments for remote quantification of trace gases, single-frequency sources, with specific tuning capabilities are required. The DIAL measurement method is based on the comparison of the optical transmission of the atmosphere for at least two consecutive wavelengths usually designated as λ_{ON}, chosen in coincidence or close to a targeted gas species absorption line, and λ_{OFF}, emitted out of resonance and close to an absorption minimum. For applications such as atmospheric greenhouse gases concentration measurements, these wavelengths are generally required to be emitted in the near or mid-infrared with a sufficiently narrow linewidth typically smaller than a few 100 MHz in order to sample the pressure broadened absorption lines [1, 2].

Another highly sought and hard to achieve key property is the capacity to switch rapidly from one wavelength to another in order to satisfy the assumption of equivalent backscattering coefficient for the consecutive emitted wavelengths used in the DIAL method. Ultimately the wavelength switching sequence should be faster than the coherence time of the atmosphere limited by the turbulence, which ranges in the few milliseconds [3]. The strategies to reach kHz or higher wavelength switching rates are essentially constrained by the technological choices for the laser source and the method used to interleave the different wavelengths. For DIALs the most general approaches consist in either using high energy ($>$ 10 mJ) – low repetition rate ($<$ few 100 Hz) Q-switched lasers with multiple pulses (corresponding to ON and OFF DiAL wavelength), or in using lower energies ($<$ few mJ) – high repetition rate ($>$ 1 kHz) sources. In the first case, peak powers can exceed hundreds of kilowatts which is very favorable for long range applications, but the spectral versatility is mostly limited to a very few number of wavelengths [4–6]. In the high repetition rate case, a lower peak power can be balanced by more versatility like fast multiple wavelengths operation [7, 8]. One important motivation for multiple-wavelengths sources is to get access to multiple molecules concentrations within the same observation frame, which can be useful to limit biases on mixing ratio retrievals [5, 9], or to increase the retrieval sensitivity by probing the absorption line of interest with a larger number of samples [10, 11].

For the laser sources, multi-wavelengths schemes are based on a variety of techniques consisting in either combining single frequency lasers with electro-optic switches in order to injection seed pulsed laser and OPO cavities [4, 12, 13], current scanning of a single seeder [7, 14–16], electro-optic modulation and filtering of a single seeder [9], or no-seeder cavity mode filtering controlling with piezo-electric transducers [17]. These last two

⋆ *E-mail:* xavier.delen@institutoptique.fr

approaches consequently result in relatively simplified and robust implementations. Single seeder scanning approaches also allows reduced alignment and cavity length control requirements [15, 18].

In this paper we propose to use parametric conversion for pulsed multiple wavelengths generation in the mid-infrared, with a slightly different approach where fast tunability is provided by a high energy narrow linewidth near infrared pump laser. The principle is to use this tunable laser to pump an OPA stage seeded by a broadly but slowly tunable pulsed OPO. The fast tunability of the pump laser can then be directly transferred to the signal or idler wave generated by the OPA and thus unlock DIAL system functionalities such as adaptation of the emitted wavelength sequence to varying environments or gas concentration ranges and dynamics [19, 20].

Pump tuned parametric devices have been previously demonstrated and used for spectrometry application but essentially in CW or quasi-CW regimes [21–23], less suitable for remote sensing. In order to go beyond and be able to carry out DIAL measurement over 1 km distance, it is required to have a rapidly tunable high peak-power pulsed laser with narrow spectral linewidth.

As a pre-requisite for a future DIAL system, we have specifically developed a pump laser providing tunable multi-mJ pulses (up to 3.5 mJ) at a high repetition frequency (5 kHz), and with a narrow spectral linewidth. This pump laser is based on a hybrid Master Oscillator Power Amplifier (MOPA) architecture, which combines fibered and bulk ytterbium amplifiers. The hybrid architecture takes advantage of *i)* the wavelength agility of fiber amplifiers, where fast wavelength scanning is supported by an externally modulated seed laser, *ii)* the pulse and repetition frequency active shaping with acousto-optic intensity modulation, and *iii)* the high energy storage capability provided by solid state lasers amplifiers. Taking advantage of the large emission bandwidth of Ytterbium doped laser materials, the high power pulsed output could be continuously tuned across a broad frequency range (up to 230 GHz in the reported set-up) through seeder modulation at the MOPA input. Finally, the high output beam quality makes this MOPA laser source ideal for down conversion pumping application in order to reach the 1.5 – 4 µm range. To illustrate this purpose the hybrid source was used to pump an OPA seeded with the 3 µm idler beam from a nested cavity optical parametric oscillator. The pump wavelength tuning was then directly transferred to the signal wave at the OPA output, which could be used to probe the absorption spectrum of an acetylene gas cell.

2 Hybrid MOPA fiber/bulk laser

A hybrid fiber/bulk architecture, in MOPA (Master Oscillator Power Amplifier) configuration, based on ytterbium-doped materials has been developed (Fig. 1). As in [24, 25], the driving idea is to take benefit from the advantages of both fiber and bulk architectures. Single-mode fiber amplifiers are particularly interesting because they offer the possibility of high gain, high compactness and robustness. Nevertheless, fiber amplifiers are largely limited by Stimulated Brillouin Scaterring (SBS) with high peak powers pulses and narrow emission linewidth (< 50 MHz). Thus, amplification in single-mode optical fibers has been maximized until the onset of this nonlinear effect. The last amplification stages were based on Yb:YAG crystals, as this material has a much higher Brillouin threshold mainly due to the larger beam sizes, the shorter propagation length and the lower Brillouin gain coefficient.

In this system, the seed source is a commercial fiber laser (Koheras BASIK Y10) at 1.03 µm delivering a continuous wave (CW) power of 10 mW. Its fast tunability can reach 10 GHz with 3 dB cut-off at 200 Hz, and its slow one can reach 0.70 nm (200 GHz). An optical isolator is placed for safety directly at the output of this laser. A double pass configuration is used for the first fiber amplifier. After passing through a circulator, the signal is first amplified in CW in a 6 µm core diameter, 1.3 m long single mode Yb-doped fiber. The pump diodes used are single mode, fiber Bragg grating stabilized, laser diodes delivering up to 700 mW at 976 nm.

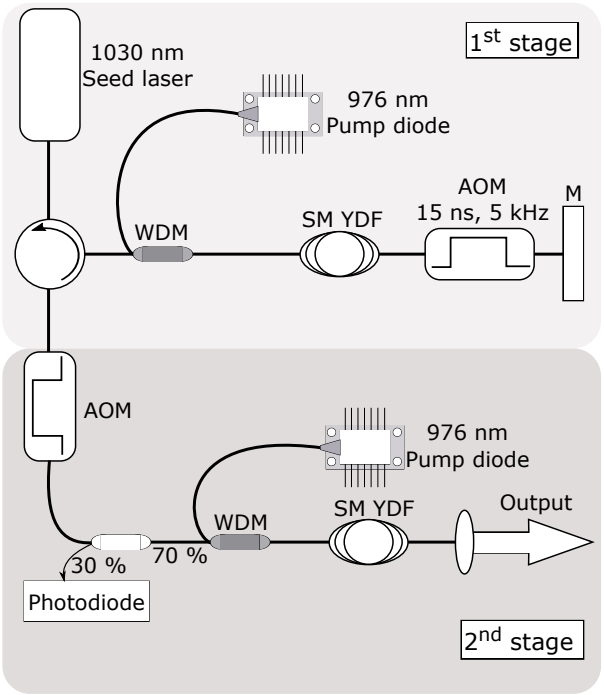

Fig. 1 Schematic diagram of the fiber amplifier. AOM, acousto-optic modulator; WDM, wavelength division multiplexer; YDF, Yb-doped fiber; M, Mirror.

At the output of the first amplifying fiber, an acousto-optic modulator (AOM) is placed to generate pulses and

a mirror is used to get a second pass. The opening time of the AOM, in double pass configuration, is defined by the round-trip time of the photons between the first and the second pass through the AOM, i.e. $t_{AR} = 2d/nc + \tau$, with τ the desired pulse duration, d the propagation distance, n the refractive index of the fiber and c the light velocity.

With the duty cycle, the average signal power after the AOM is strongly reduced by about 47 dB, including transmission losses. An average power in the µW range returns to the fiber amplifier at the input of the second pass. The signal is extracted by the circulator after two passes in the active fiber. The average input power being much lower at the second pass than at the first pass, the return of the pulse signal back into the fiber does not change the inversion of population along the fiber. Thus, the gain in the fiber is established by the first pass and is reused by the second pass. Figure 2 shows the output pulse energy and peak power versus the seed power in CW. The energy at the output of the double pass increases when the seed power is reduced, which might seem counterintuitive at first sight. This is due to the lower gain saturation in the first pass where the seed is CW, leading to a higher pulse energy at the overall two-pass amplifier output.

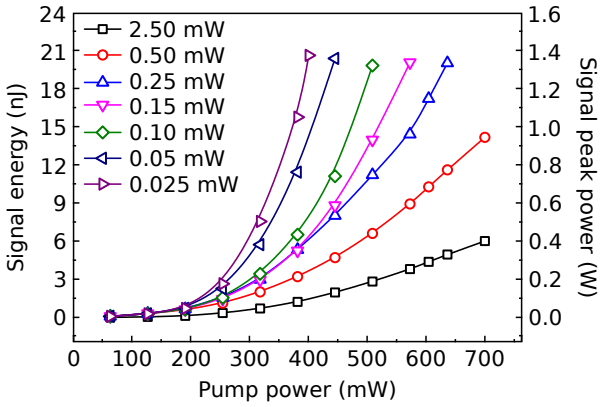

Fig. 2 Amplified laser pulse energy (left axis) and peak power (right axis) versus incident pump power.

With this configuration, energies of 20 nJ have been obtained, i.e. a peak power of 1.3 W. The second fiber amplifier is expected to be limited by SBS. For a fiber, the power threshold for SBS can be written as [26–28]:

$$P_{th} = 21 \frac{A_{eff}}{g_b L_{eff}} \quad (1)$$

where A_{eff} is the effective fiber area, g_b the Brillouin gain and L_{eff} the effective fiber length. This effective length depends on the gain or losses in the fiber. For a gain G much larger than 1 in an amplifying fiber, the relation (1) can be rewritten [29]:

$$P_{th} = 21 \frac{A_{eff} \ln(G)}{g_b L} \quad (2)$$

Although this result is approximate because it assumes a constant gain along the fiber, it shows that a higher SBS threshold can be obtained with a high gain short fiber. The output peak power can thus be maximized by searching for the optimum fiber length. If too long, the low linear gain close to the fiber output will result in a lower SBS threshold. However, if the fiber is too short, the overall gain might be too small to reach the SBS limit. To search for the optimum fiber length experimentally, we monitored the back scattered SBS pulse using a fiber coupler.

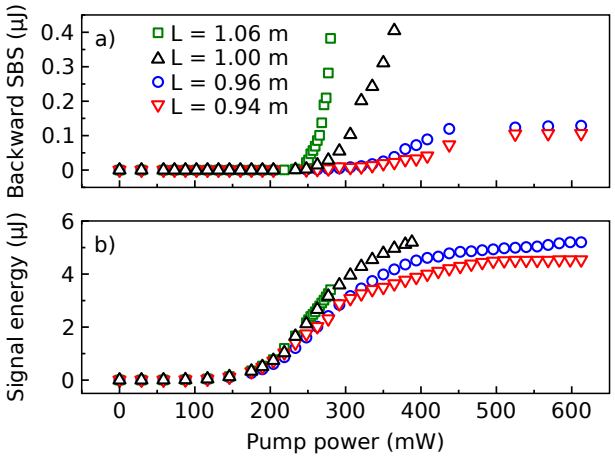

Fig. 3 For different lengths of doped fiber. **(a)** Brillouin power measured at the oscilloscope as a function of pump power. **(b)** Signal energy as a function of pump power.

Figure 3 shows the evolution of the output signal energy (Fig. 3b) and the power backscattered by the SBS and amplified in the fiber (Fig. 3a) as a function of the pump power. The results are presented for four different fiber lengths and allow to adjust experimentally the optimal length. The length of the fibers differed by only 12 cm between the maximum and minimum length. With the 1.06 m fiber (blue squares), the signal and SBS power increase very rapidly, up to pumping powers of 300 mW (limited at this level for component safety). The output energy is then of 3.2 µJ. By shortening the fiber by 10 cm (black rounds), the saturation of the pump absorption results in a saturation of the output power versus the pump power. It indicates that the linear gain is still high at the output, which results in a higher SBS threshold. It is then possible to obtain an output energy of 5 µJ corresponding to a peak power of over 330 W. This study shows the importance of taking into account the SBS to evaluate the optimum fiber length for the amplifier.

To reach higher energies of the order of mJ, two Yb:YAG based amplification stages were placed at the output of these fiber stages. The crystals used have a doping of 1.5% and dimensions of 2 × 8 × 17 mm^3. Similar double-pass amplifier architectures have already

been described in previous work [30–33].The first stage is optimized to maximize the gain whereas the second stage is designed to extract high output energies.

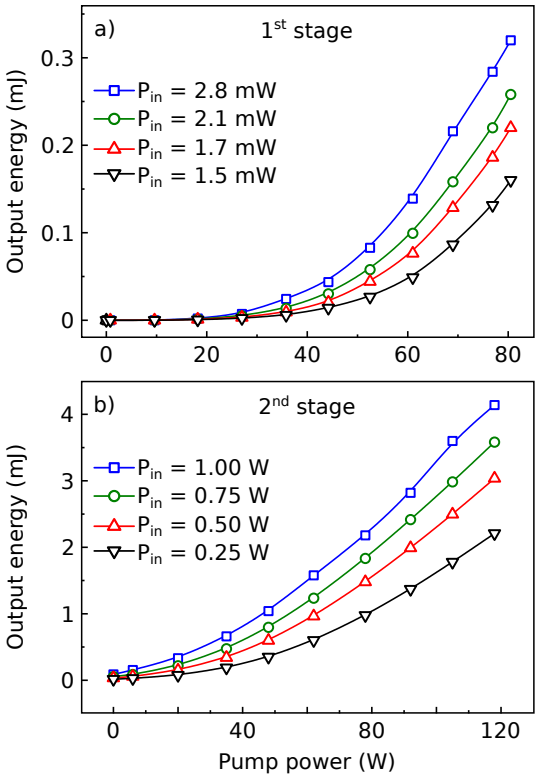

Fig. 4 **(a)** Signal energy at the output of the first amplification stage and beam profile. **(b)** Signal energy at the output of the second amplifier stage.

Figures 4a and b show the evolution of the output energy of the first and second amplifiers versus the pump power for different seed power levels. An output energy per pulse of 3 mJ at 5 kHz was measured without significant degradation of the beam profile, with an $M^2 < 1.2$ (Fig. 5a). The anti-reflective coating of the crystal of the second amplifier was damaged at an output energy higher than 3.7 mJ for a signal beam waist of 200 µm. The Fig. 5b shows the temporal profile of the 15 ns pulse at the laser output. We observe a slight modulation in the pulse (at around 500 MHz) due to parasitic reflections into the first stage of fiber amplification.

3 Parametric conversion towards near and mid-infrared and potential for future DIAL emitters

To show the potential of this laser for frequency conversion to the near or mid-infrared by a non-linear stage, we used this hybrid laser as a pump for an OPA stage.

The OPA is seeded by a Nested Cavity OPO (NesCOPO) pumped by a wavelength-controllable, commercial fiber laser emitting at 1.064 µm [34, 35]. The

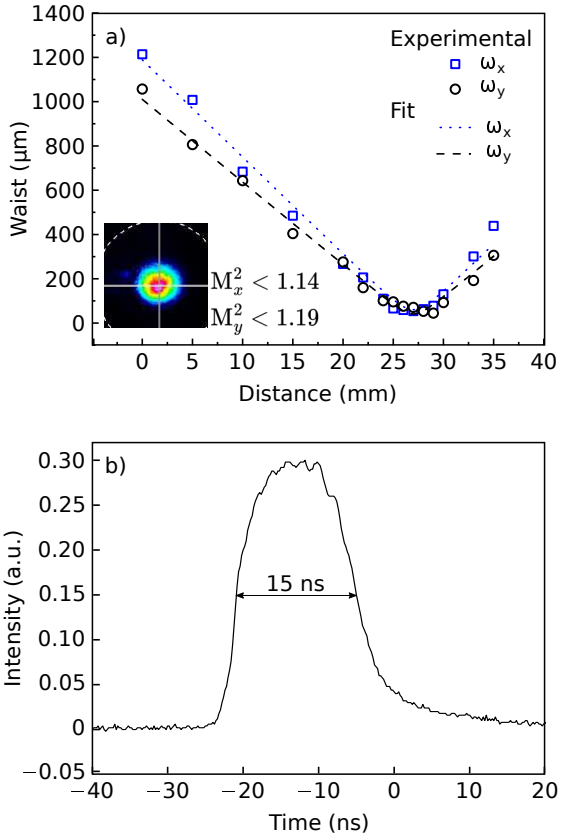

Fig. 5 **(a)** Measurement of the caustic and the spatial profile of the signal beam at full power at the output of the double pass amplification. **(b)** Time measurement recorded for a laser output power of 3W.

pump pulses have a duration of 320 ns at a repetition rate of 5 kHz, with a maximum energy of 30 µJ. The NesCOPO crystal is a 4 mm long periodically-poled Lithium Niobate (PPLN) crystal. Several gratings are inscribed on the crystal, allowing to produce radiation in the 3.2-3.7 µm range. For the following tests, the idler emission of the OPO was set in the 3.2 µm range. The maximum measured energy for the single frequency idler wave is 0.7 µJ at 3.2 µm.

The wavelength of the NesCOPO is measured using a wavemeter, and a control loop is implemented to lock its emitted frequency.

The overall experiment is shown in Fig. 6. The idler wave is injected into a sequence of 3 PPLN crystals of 34, 25 and 13 mm length respectively, pumped by the hybrid laser described above. The 2 mm thickness of these crystals limits the maximum incident pump energy to 1 mJ, to avoid damages on the crystal facets. Such limitation could be loosened by the use of higher aperture PPLN crystals, which are now commercially available.

With a maximum pump energy of 1 mJ and a waist of 350 µm for each beam, a maximum energy of 150 µJ was measured for the signal (λ_s OPA) at the output of the OPA. Further improvement of the OPA set-up, with longer crystals, an idler filtering between the crystals

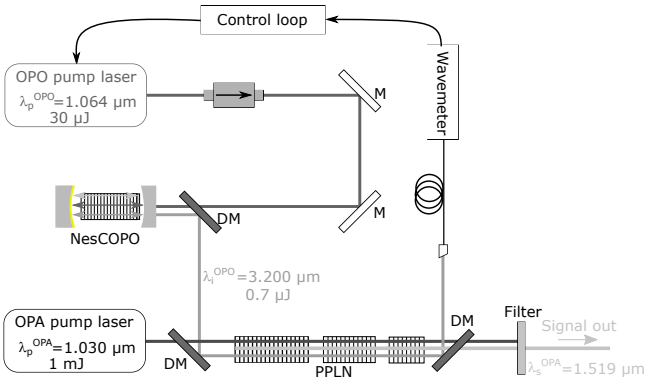

Fig. 6 Overall parametric frequency conversion set-up. DM, dichroic mirror; M, mirror.

and with a better temporal overlap of the pump and idler waves, could lead to an even higher conversion efficiency.

Given that the OPO idler beam seeds the OPA at a fixed and stabilized wavelength, the signal wavelength of the OPA (λ_s OPA) can be tuned by tuning the pump laser wavelength. This is shown on Fig. 7 for two different modes of operation of the hybrid pump laser. In a first slow mode (Fig. 7a), the temperature of the 1030 nm fiber seed laser is adjusted to cover a 0.7 nm range(200 GHz) to tune the λ_s OPA over around 1.7 nm. In a faster and finer wavelength tuning mode (Fig. 7b), the hybrid pump laser wavelength seeder is adjusted by playing on the voltage through a piezoelectric transducer. Thus, it can generate rapid tuning scan over 10 GHz, which could be of high interest for DIAL, allowing to generate $\lambda_{ON}/\lambda_{OFF}$ wavelengths sequences, with arbitrary positions over an absorption line.

Such a prospect is illustrated by scanning the absorption lines of an acetylene cell. The signal wave generated in these OPA stages is partially coupled in a 50/50 fibered beam splitter. One part is directly connected to a photodiode, the other part passes through the acetylene-filled cell and is coupled to another photodiode, allowing to measure the cell transmission. The cell is 3 cm long and filled with 100% acetylene at a pressure of 200 Torr.

The points in Fig. 8 are experimental data and the line is a theoretical curve calculated using HITRAN database [36]. For each point, we observe a signal fluctuation of 3 to 5% represented by the vertical error bars. The wavelength error is mostly dominated by the resolution of the 200 MHz lambdameter and those of the pump wavelength, i.e. an error of 0.02 nm.

In the future, using the NesCOPO signal instead of the idler, and combining the coarse wavelength tuning of the NesCOPO over several hundreds of nm, with the fine and easy tuning of the hybrid pump laser, could thus allow scanning of absorption lines in the 3.2-3.7µm region, where most molecules of interest display strong absorption lines. Such OPA scheme could also be envisioned using other seed devices than a NesCOPO, as a single frequency laser diode, which would reduce the tunability, but further simplify the set-up.

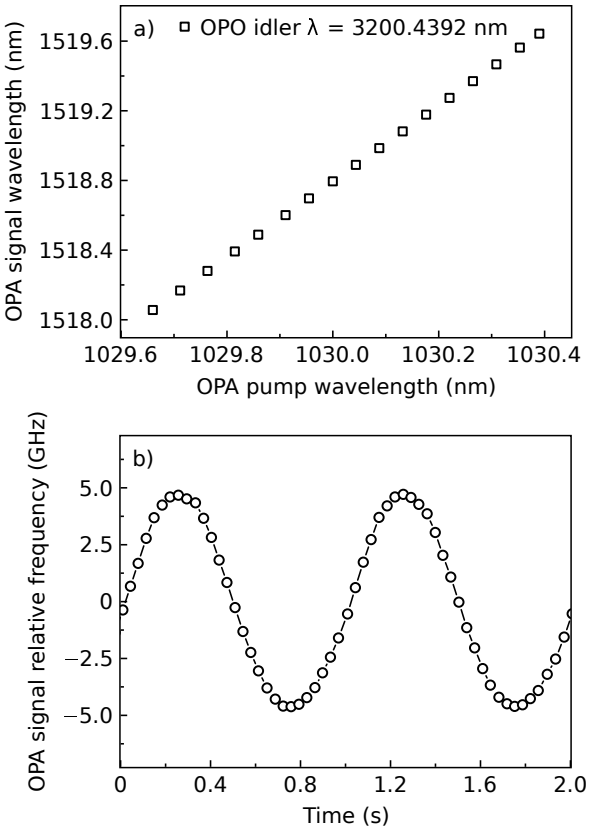

Fig. 7 Wavelength of the signal wave (recorded with a wavemeter) from the OPA as a function of the wavelength of the OPA pump, for a fixed wavelength OPO idler wave. The left figure **(a)** corresponds to a coarse, slow temperature tuning of the hybrid laser seeder. The right figure **(b)** is obtained for a fast tuning of the hybrid laser seeder (1Hz frequency tuning speed, limited by the wavemeter acquisition time).

4 Conclusion

We reported on a high power, 5 kHz, 1030 nm, wavelength agile hybrid fiber-bulk laser, emitting up to 3 mJ of pulse energy in the nanosecond regime. This hybrid laser is based on a commercial seed fiber laser, whose wavelength is tunable over several GHz, amplified in a dual-stages Ytterbium doped single-mode fiber amplifier, followed by two Yb:YAG bulk amplifiers. In order to demonstrate the potential of such an architecture for future differential absorption LIDAR emitters, this hybrid source was used to amplify a single frequency, nested cavity, optical parametric oscillator, emitting a fixed wavelength in the 3 µm region, within an OPA set-up. Wavelength tuning of the hybrid pump allowed to tune the emission of the OPA generated signal wave, showing interesting potential for DIAL emitters.

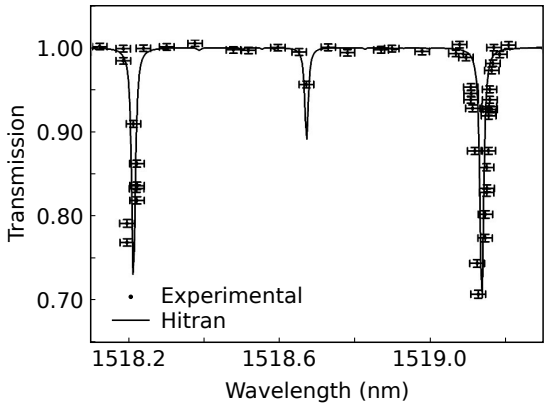

Fig. 8 Absorption measurement of acetylene as function of the emitted OPA signal wavelength, tuned by tuning the frequency of the hybrid pump laser. Points represent experimental data and the line is a calculation from HITRAN database [36]

Such a pump laser tuning scheme could also be envisioned using other seed devices, as a laser diode, in order to further simplify the set-up. This pump could also be used for direct pumping of innovative OPO architectures, such as backward OPO, which also allows no-seeder narrow linewidth emission in the pulsed regime and could benefit from pump tuning.

Funding

This work is supported by "Investissements d'Avenir" LabEx PALM (ANR-10-LABX-0039-PALM)

Acknowledgement

The authors are thankful to Kjell Martin Mølster from Department of Applied Physics, Royal Institute of Technology (KTH), Stockholm (Sweden), for helpful discussion about the laser linewidth.

References

[1] R. Bogue. Sens. Rev. **35**, 133 (2015).
[2] B. J. Orr. *Encyclopedia of Analytical Chemistry*. Ed. by R. A. Meyers. Chichester, UK: John Wiley & Sons, Ltd, 2017, pp. 1–49.
[3] N. Menyuk and D. K. Killinger. Opt. Lett. **6**, 301 (1981).
[4] F. Gibert, J. Pellegrino, D. Edouart, C. Cénac, L. Lombard, J. Le Gouët, T. Nuns, A. Cosentino, P. Spano, and G. Di Nepi. Appl. Opt. **57**, 10370 (2018).
[5] T. F. Refaat, U. N. Singh, J. Yu, M. Petros, S. Ismail, M. J. Kavaya, and K. J. Davis. Appl. Opt. **54**, 1387 (2015).
[6] T. F. Refaat, M. Petros, U. N. Singh, C. W. Antill, R. G. Remus, and S. Ismail. IGARSS 2019. Yokohama, Japan: IEEE, 2019, pp. 4861–4864.
[7] J. Abshire, A. Ramanathan, H. Riris, J. Mao, G. Allan, W. Hasselbrack, C. Weaver, and E. Browell. Remote Sensing **6**, 443 (2013).
[8] G. A. Wagner and D. F. Plusquellic. Appl. Opt. **55**, 6292 (2016).
[9] G. A. Wagner and D. F. Plusquellic. Opt. Express **26**, 19420 (2018).
[10] J. R. Chen, K. Numata, and S. T. Wu. Opt. Express **27**, 36487 (2019).
[11] G. Han, H. Xu, W. Gong, X. Ma, and A. Liang. Appl. Opt. **56**, 8532 (2017).
[12] K. Ertel, H. Linné, and J. Bösenberg. Appl. Opt. **44**, 5120 (2005).
[13] K. Numata, S. Wu, and H. Riris. Appl. Phys. B **116**, 959 (2014).
[14] K. Numata, H. Riris, S. Li, S. Wu, S. R. Kawa, M. Krainak, and J. Abshire. J. Appl. Remote Sens **6**, 063561 (2012).
[15] H. Riris, K. Numata, S. Wu, B. Gonzalez, M. Rodriguez, S. Scott, S. Kawa, and J. Mao. J. Appl. Remote Sens **11**, 034001 (2017).
[16] Y. Shibata, C. Nagasawa, and M. Abo. Appl. Opt. **56**, 1194 (2017).
[17] A. Godard, M. Raybaut, and M. Lefebvre. *Encyclopedia of Analytical Chemistry*. Ed. by R. A. Meyers. Chichester, UK: John Wiley & Sons, Ltd, 2017, pp. 1–35.
[18] M. Stephen, A. Yu, J. Chen, K. Numata, S. Wu, B. Gonzales, L. Han, M. Fahey, M. Plants, M. Rodriguez, G. Allan, J. Abshire, J. Nicholson, A. Hariharan, W. Mamakos, and B. Bean. Components and Packaging for Laser Systems IV. **10513**. San Francisco, United States: SPIE, 2018, p. 1051308.
[19] J. Hamperl, C. Capitaine, J.-B. Dherbecourt, M. Raybaut, P. Chazette, J. Totems, B. Grouiez, L. Régalia, R. Santagata, C. Evesque, J.-M. Melkonian, A. Godard, A. Seidl, H. Sodemann, and C. Flamant. Atmos. Meas. Tech. **14**, 6675 (2021).
[20] M. Wirth, A. Fix, P. Mahnke, H. Schwarzer, F. Schrandt, and G. Ehret. Appl. Phys. B **96**, 201 (2009).
[21] J. Courtois, R. Bouchendira, M. Cadoret, I. Ricciardi, S. Mosca, M. De Rosa, P. De Natale, and J.-J. Zondy. Opt. Lett. **38**, 1972 (2013).
[22] I. D. Lindsay, B. Adhimoolam, P. Groß, M. E. Klein, and K.-J. Boller. Opt. Express **13**, 1234 (2005).
[23] M. Vainio, J. Peltola, S. Persijn, F. J. M. Harren, and L. Halonen. Opt. Express **16**, 11141 (2008).
[24] R. Zhu, J. Wang, J. Zhou, J. Liu, and W. Chen. Appl. Opt. **51**, 3826 (2012).
[25] X. Délen, L. Deyra, A. Benoit, M. Hanna, F. Balembois, B. Cocquelin, D. Sangla, F. Salin, J. Didierjean, and P. Georges. Opt. Lett. **38**, 995 (2013).

[26] M. Niklès, L. Thevenaz, and P. A. Robert. J. Lightwave Technol. **15**, 1842 (1997).
[27] G. P. Agrawal. *Nonlinear fiber optics*. Fifth edition. Amsterdam: Elsevier/Academic Press, 2013, pp. 355–388.
[28] A. Yeniay, J.-M. Delavaux, and J. Toulouse. J. Lightwave Technol. **20**, 1425 (2002).
[29] J. W. Dawson, M. J. Messerly, R. J. Beach, M. Y. Shverdin, E. A. Stappaerts, A. K. Sridharan, P. H. Pax, J. E. Heebner, C. W. Siders, and C. Barty. Opt. Express **16**, 13240 (2008).
[30] F. Lesparre, I. Martial, J. Didierjean, J. T. Gomes, W. Pallmann, B. Resan, A. Loescher, J.-P. Negel, T. Graf, M. Abdou Ahmed, F. Balembois, and P. Georges. SPIE LASE - Solid State Lasers XXIV: Technology and Devices. Ed. by W. A. Clarkson and R. K. Shori. **9342**. San Francisco, California, United States: SPIE, 2015, p. 934203.
[31] F. Lesparre, J. T. Gomes, X. Délen, I. Martial, J. Didierjean, W. Pallmann, B. Resan, M. Eckerle, T. Graf, M. Abdou Ahmed, F. Druon, F. Balembois, and P. Georges. Opt. Lett. **40**, 2517 (2015).
[32] F. Lesparre, J. T. Gomes, X. Délen, I. Martial, J. Didierjean, W. Pallmann, B. Resan, F. Druon, F. Balembois, and P. Georges. Opt. Lett. **41**, 1628 (2016).
[33] F. Lesparre, J. T. Gomes, X. Délen, I. Martial, J. Didierjean, W. Pallmann, B. Resan, M. Eckerle, T. Graf, M. Abdou Ahmed, F. Druon, F. Balembois, and P. Georges. Advanced Solid State Lasers. Berlin: OSA, 2015, AW3A.9.
[34] J. B. Barria, S. Roux, J.-B. Dherbecourt, M. Raybaut, J.-M. Melkonian, A. Godard, and M. Lefebvre. Opt. Lett. **38**, 2165 (2013).
[35] G. Aoust, A. Godard, M. Raybaut, J.-B. Dherbecourt, G. Canat, and M. Lefebvre. J. Opt. Soc. Am. B **31**, 3113 (2014).
[36] L. Rothman, I. Gordon, A. Barbe, D. Benner, P. Bernath, M. Birk, V. Boudon, L. Brown, A. Campargue, J.-P. Champion, K. Chance, L. Coudert, V. Dana, V. Devi, S. Fally, J.-M. Flaud, R. Gamache, A. Goldman, D. Jacquemart, I. Kleiner, N. Lacome, W. Lafferty, J.-Y. Mandin, S. Massie, S. Mikhailenko, C. Miller, N. Moazzen-Ahmadi, O. Naumenko, A. Nikitin, J. Orphal, V. Perevalov, A. Perrin, A. Predoi-Cross, C. Rinsland, M. Rotger, M. Šimečková, M. Smith, K. Sung, S. Tashkun, J. Tennyson, R. Toth, A. Vandaele, and J. Vander Auwera. J. Quant. Spectrosc. Radiat. Transf. **110**, 533 (2009).